Charge Transfer and Transport in Polymer-Fullerene Solar Cells

J. Parisi, V. Dyakonov, M. Pientka, I. Riedel, C. Deibel, C. J. Brabec[a], N. S. Sariciftci[c], and J. C. Hummelen[c]

Faculty of Physics, Department of Energy and Semiconductor Research, University of Oldenburg, D-26111 Oldenburg

[a] Siemens AG, CT MM1 Innovative Polymers, Paul-Gossen-Straße 100, D-91052 Erlangen

[b] Institute of Physical Chemistry and Linz Institute of Organic Solar Cells, University of Linz, Altenberger Straße 69, A-4040 Linz

[c] Stratingh Institute and Materials Research Center, University of Groningen, Nijenborgh 4, NL-9747 AG Groningen

Reprint requests to Prof. J. P.; Fax: +49 (0)441 798-3326; E-mail: parisi@ehf.uni-oldenburg.de

The development of polymer-fullerene plastic solar cells has made significant progress in recent years. These devices excel by an efficient charge generation process as a consequence of a photo-induced charge transfer between the photo-excited conjugated polymer donor and acceptor-type fullerene molecules. Due to the paramagnetic nature of the radical species, the photo-induced charge transfer can be analyzed by the help of light-induced electron spin resonance spectroscopy. Upon looking at an interpenetrating donor-acceptor composite consisting of the polymer MDMO-PPV and the fullerene derivative PCBM, we disclose two well separated line groups having a strongly anisotropic structure. The line shape can be attributed to an environmental axial symmetry of the polymer cation and a lower rhombohedric symmetry of the fullerene anion. Since the signals were found to be independent of one another with different spin-lattice relaxation times, the radical species can be discriminated via separate characterization procedures. In order to study the bulk charge transport properties, we carried out admittance spectroscopy on the polymer-fullerene solar cell device including a transparent semiconductor oxide front contact (ITO/PEDOT:PSS) and a metal back contact (Al). The temperature- and frequency-dependent device capacitance clearly uncovers two different defect states, the first, having an activation energy of 9 meV, indicates a shallow trap due to a bulk impurity, the latter, having an activation energy of 177 meV, can be assigned to an interfacial defect state located between the polymer-fullerene composite and the metal back contact.

Key words: Organic Solar Cell; Fundamentals; Characterization.

1. Introduction

Conjugated polymers are well known as intrinsic, quasi-one-dimensional semiconductors with band gap energies covering the whole visible range of photon wavelengths [1]. Their application in opto-electronic devices like organic light emitting diodes (OLEDs) has already reached the state of an industrial low-cost fabrication. However, the performance of photovoltaic devices with a light absorber consisting only of a single-type conjugated polymer is comparably poor, due to the low photo-generation yield, the strong radiative recombination, and the low mobility of the charge carriers [2].

In 1992, Sariciftci *et al.* [3] demonstrated that doping of several conjugated polymers with fullerenes, C_{60}, results in a strong quenching of photoluminescence. Furthermore, it has been observed that the photocurrent of solar cell devices, which have an absorber of a conjugated polymer, increases by nearly two orders of magnitude when fullerenes are embedded in the photo-active film. The underlying photophysics may be described by a light-induced, ultrafast formation of an ion-radical pair, i. e. a polymer cation, P^+, and the fullerene anion C_{60}^-. This reaction is better known as the ultrafast photo-induced charge transfer, similar to one of the early steps in natural photosynthesis.

Due to the non-compensated spins and their resulting magnetic moments, the reaction products can be discriminated by means of paramagnetic resonance techniques, like electron spin resonance (ESR) spec-

troscopy. However, no resonant signals were found for polymer-fullerene composites in the dark, underlining that the focussed process occurs only upon light excitation of the polymer moiety [3, 4]. We applied light-induced electron spin resonance (LESR) on blends of the conjugated polymer MDMO-PPV (poly-[(2-methoxy-5-(3-,7-dimethyl-octyloxy)-1,4 phenylene vinylene]) and the soluble methanofullerene PCBM ([6,6] phenyl-C_{61}-butyric acid methyl ester), in order to study the charge separated state.

A promising device configuration for polymer-fullerene solar cells is given by the concept of a bulk heterojunction: A thin polymer-fullerene composite layer is sandwiched between two electrodes with differing work functions, giving rise to an electrical built-in field. For the particular donor-acceptor pair MDMO-PPV: PCBM, power conversion efficiencies of 2.5 % under white light AM 1.5 conditions have been demonstrated [5]. We prepared similar devices with identical materials, in order to study the transport properties of these bi-continuous networks. If the photo-generated charge carriers were trapped by defect states, this would contribute to the device capacitance and could be studied by means of admittance spectroscopy. From these measurements, the activation energy E_A, the capture cross-section σ_h, and the emission time τ can be derived. Furthermore, a modification of the measurement allows to distinguish between bulk defects and such traps, which are situated at interfacial layers, i.e. at the bulk-electrode interface.

2. Experimental Details

For device preparation we use carefully cleaned glass substrates, partially coated with indium tin oxide (ITO). Since the surface quality, i. e. the roughness, strongly depends on the production method, a thin layer of the p-conducting conjugated polymer PEDOT:PSS (poly-[ethylene dioxy thiophene]:poly-[styrene sulphonic acid]), obtained from Bayer AG, is introduced to even the electrode surface and to avoid shorts. PEDOT:PSS is spin cast from a water based solution. Subsequently, residual water is removed either in a vacuum chamber or by heating. The substances which form the photo-active layer, i. e. MDMO:PPV and PCBM, are dissolved separately in chlorobenzene and mixed afterwards in the desired ratio of 1:3. The composite solution is applied by spin coating in a dry nitrogen atmosphere. The aluminum rear electrode
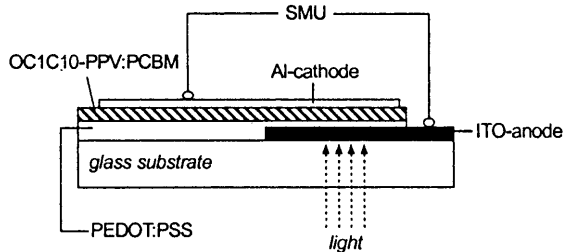

Fig. 1. Device configuration for a bulk-heterojunction photovoltaic device with the structure ITO/PEDOT:PSS/MDMO-PPV:PCBM/Al.

is subsequently thermally evaporated in a vacuum chamber at pressures between 10^{-6} to 10^{-7} mbar. Figure 1 shows the schematic device configuration. For LESR measurements, Bruker X-band (9.5 GHz) and W-band (95 GHz) spectrometers have been used. The devices were placed in a variable temperature cryostat and excited by the 488 nm line of an Ar^+ laser.

Admittance spectroscopy was carried out in a He closed cycle cryostat in the temperature range from 20 K to 300 K using a Solartron 1260A impedance analyzer, equipped with a dielectric interface (Solartron 1296A). To work close to equilibrium, only a small AC signal amplitude of 30 mV was chosen.

3. Results and Discussion

When ESR is carried out on MDMO-PPV:PCBM blends in the dark, no resonant signals are obtained in an inert gas atmosphere. This has been established for different composites, too. In contrast, we have detected two separate contributions in the LESR spectrum, i.e. under photoexcitation, when working in conventional X-band at a microwave frequency of 9.5 GHz. The condition for paramagnetic resonance is given by

$$g = h\nu/\mu_B B, \tag{1}$$

where g is the g-factor, h Planck's constant, ν the frequency of the microwave, μ_B the Bohr magnetron, and B the magnetic field strength. The detected lines are located at the g-factors $g_1 = 2.0025$ and $g_2 = 1.9995$, where g_1 is attributed to the positive polaron P^+, i. e., the polymer cation, and the latter one to the fullerene anion. (The deviation of g from the value 2.0023 originates from a non-zero orbit momentum.) However, both signals show a strong overlap, which
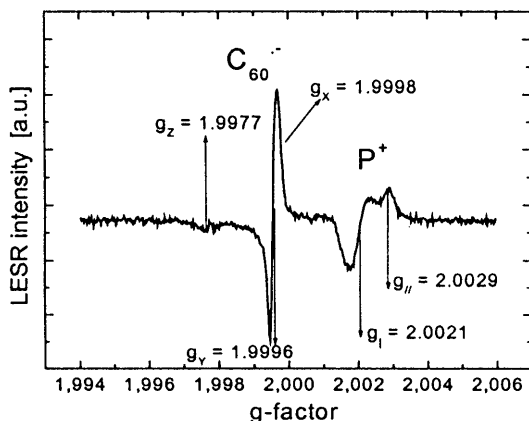
Fig. 2. W-band LESR spectrum for a composite of MDMO-PPV and PCBM. Two different line groups are resolved and attributed to the polymer cation P^+ and to the anion of the C_{60} derivative PCBM.

Fig. 3. ESR spectrum of iodine-doped MDMO-PPV, represented as a function of the magnetic field B. The signal Mn^{2+} was used for calibration.

prevents a separate study of the different resonances. In addition, a possible g-factor anisotropy cannot be resolved. Hence, we carried out LESR in the W-band at 95 GHz microwave frequency and approximately ten times higher magnetic field strengths, which can be calculated from the resonance condition, see (1).

W-band LESR spectroscopy allows one to resolve overlapping signals, on the one hand, and to detect hidden structures within each group of lines, on the other hand. Figure 2 displays the W-band LESR spectrum for an MDMO-PPV:PCBM sample. One can clearly distinguish between the two signals of the polymer cation and the fullerene anion. Furthermore, the anisotropy of the g-factor is fully resolved.

The signal for the polymer cation, i. e. the polaron P^+, can be simulated by iodine doping of the pristine MDMO-PPV. Figure 3 displays the dark-ESR spectrum of MDMO-PPV:I_2 in the W-band, which is nearly identical to the positive polaron signal which has been obtained for the blend under illumination (see Figure 2).

In case of the polaron P^+, two components of the g-tensor were obtained: One contribution $g_{\parallel} = 2.0029$ corresponds to a magnetic moment which has a component parallel to the external field. The second resonance, the perpendicular component, is pronounced as a "shoulder" at $g_{\perp} = 2.0021$. Both g-factors indicate an axial environmental symmetry for the polaron charge species, which can be derived from the line shape. For the fullerene anion, a lower, rhombohedric symmetry was disclosed with the contribu-
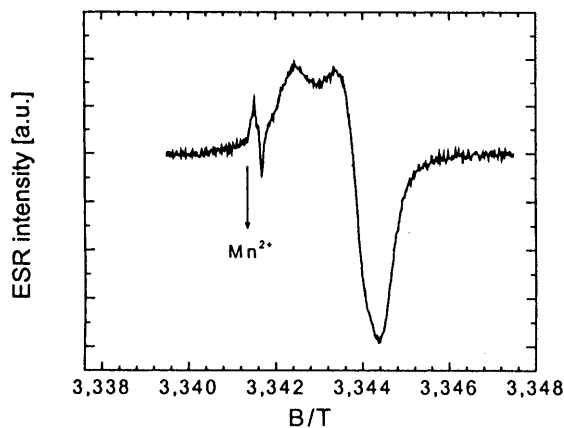
tions $g_x = 1.9998$, $g_y = 1.9996$, and $g_z = 1.9977$. We also found that both signals can be studied separately, when making use of signal saturation, due to the different spin-lattice relaxation times of the radical species. The latter proves that the photo-generated charge species are independent of each other, without any spin-exchange-type correlation effects.

If a solar cell is considered as a capacitor with the capacitance C, the complex admittance Y is given by

$$Y = G + i\omega C. \qquad (2)$$

In (2), G means the conductance, i the imaginary unit, and ω the angular frequency ($\omega = 2\pi f$, f = frequency). For a semiconductor or a solar cell, let us briefly discuss several contributions to the complex admittance. If a space charge region is apparent, thermally activated charge carriers contribute to the device admittance. If an AC voltage is applied, these charges respond at the frequency and, hence, contribute to the complex admittance, until a critical frequency ω_0 is reached. This value corresponds to the situation where the device behaves like a dielectric medium. Furthermore, trap states in the bulk or such, which are located at the interfaces, may give rise to the device capacitance by the capture or emission of free charge carriers. The characteristic features of these defect states can be derived from the $C(\omega)$ spectrum at certain critical frequencies ω_0, where an instantaneous decrease of the capacitance is observed. If we consider a defect state with the emission rate $\omega = 1/\omega_0$, the dependence of the capacitance on the
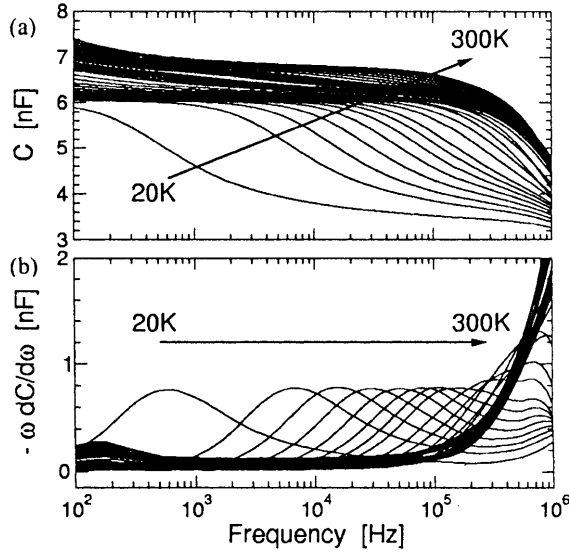
Fig. 4. (a) Frequency spectrum of the device capacitance $C(\omega)$ of an ITO/PEDOT:PSS/MDMO-PPV:PCBM/Al solar cell. The arrows indicate the direction of increasing temperature. (b) Normalized derivative $-\omega \mathrm{d}C/\mathrm{d}\omega$ of the capacitance-frequency spectrum $C(\omega)$.

frequency ω is given by [6]

$$C \propto \omega_0^2/(\omega^2 + \omega_0^2). \tag{3}$$

Equation (3) is a stepwise function, whereas the critical frequency ω_0 gives the temperature-dependent parameter:

$$\omega_0 = \tau^{-1} = N_v v_{th}\sigma_h \exp(-E_A/k_B T). \tag{4}$$

The expression reveals the activation energy E_A of the defect state and the dependence of the emission rate on temperature. In (4), N_V means the effective density of states in the valence band, v_{th} the thermal velocity of the charge carriers, and σ_h the capture cross-section for holes. Assuming that $v_{th} \propto T^{1/2}$ and $N_V \propto T^{3/2}$, one may express (4) like

$$\omega_0 = \tau^{-1} = \xi_0 T^2 \sigma_h \exp(-E_A/k_B T). \tag{5}$$

where ξ_0 means the pre-exponential factor. Upon plotting ω_0 as a function of the reciprocal temperature T^{-1} (Arrhenius representation), one can derive the activation energy from the slope. The temperature-dependent pre-exponential factor $\nu_0 = \xi_0 T^2 \sigma_h$ is then obtained from the axis cut-off $T^{-1} \to 0$ K.
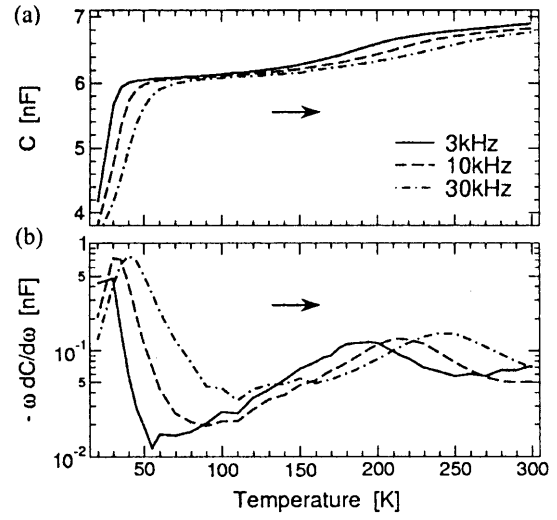

Fig. 5. (a) Capacitance C as a function of the temperature T for different frequencies. (b) Differentiated capacitance $-\omega \mathrm{d}C/\mathrm{d}\omega$ versus T for different frequencies. The arrows indicate the direction of increased frequency.

We carried out temperature-dependent admittance spectroscopy on a polymer-fullerene solar cell with the configuration ITO/PEDOT:PSS/MDMO-PPV:PCBM/Al. Figure 4 (a) displays the frequency spectra of the measured capacitance for temperatures ranging from 20 to 300 K. The arrow indicates the increase of temperature. One clearly observes a step which is shifted to higher frequencies when the temperature increases. In order to evaluate the position of the steps, it is more reasonable to plot $-\omega \mathrm{d}C/\mathrm{d}\omega$ versus ω instead of $C(\omega)$. Figure 4 (b) shows the normalized derivative of the frequency spectrum of the capacitance. The steps now appear as maxima within the single curves, and the corresponding critical frequency ω_0 can be derived more accurately. A more detailed evaluation is given by the representation of the capacitance as a function of temperature (Fig. 5(a)) or the derivation $-\omega \mathrm{d}C/\mathrm{d}\omega$ (Fig. 5(b)), respectively. In Fig. 5(a), two steps, which shift towards higher temperatures with increasing frequency, can be clearly distinguished. These two steps correspond to different defect states with characteristic activation energies.

From the data plotted in Figs. 4 and 5, we carried out an Arrhenius evaluation, like it is seen in Figure 6. For both defect states, the activation energies and the pre-exponential factors were calculated from the curves obtained. For the first trap state, a relatively small activation energy of $E_{A1} = 9$ meV and a pre-exponential
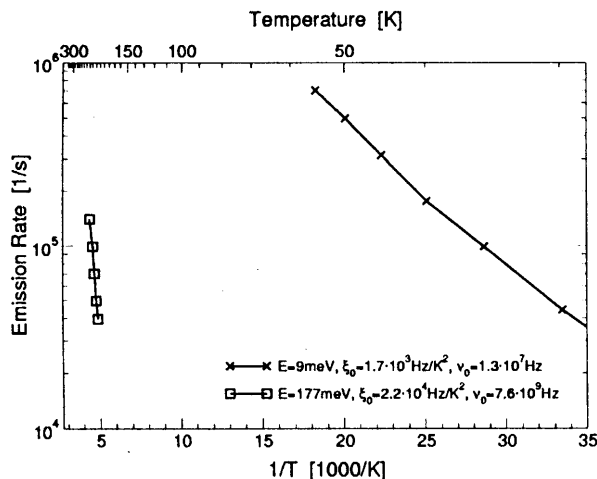
Fig. 6. Arrhenius evaluation of the admittance spectra of an ITO/PEDOT:PSS/MDMO-PPV:PCBM/Al device. Two different, frequency-dependent contributions to the device capacitance were found at activation energies $E_{A1} = 9$ meV and $E_{A2} = 177$ meV.

factor of $\xi_{01} = 1.7 \times 10^3 \, \text{s}^{-1} \text{K}^{-2}$ have been found. This state is attributed to a very shallow defect, which may contribute to the thermally activated conductivity observed. A further defect has been found at $E_{A2} = 177$ meV and $\xi_{02} = 2.2 \times 10^4 \, \text{s}^{-1} \text{K}^{-2}$. According to earlier studies, we assume that the latter originates from trapping centers at the composite-metal interface [7]. In former measurements, the corresponding step was found to be independent of a DC bias, which provides evidence for an apparent Fermi-level pinning. Since no DC-bias dependence is observed for this defect state, we rule out bulk defects: For the latter, one would expect a weak bias sensitivity due to the hopping nature of the charge transport. At high electric fields, the Coulomb barriers, which separate adjacent hopping centers, should be lowered or increased, when a DC voltage is applied (Poole-Frenkel mechanism). The latest measurements revealed a DC-bias independent behavior of the shallow activation center.

4. Conclusions

By means of W-band LESR spectroscopy, we are able to follow the formation of ion radicals, generated due to the photo-induced charge transfer in polymer-fullerene composites. Working in the W-band enables us to resolve the hidden structure of the line groups, which were obtained from X-band measurements. The spectrum in Fig. 2 exhibits two clearly distinguishable groups of lines, which can be attributed to the fullerene anion ($g < 2$) and to the polymer cation P^+ ($g > 2$). The latter has been independently identified by the dark-ESR spectrum for iodine-doped, pristine MDMO-PPV (Fig. 3). A strong anisotropy of the splitting factor is obvious: Three different components of the g-tensor are derived from the line group of PCBM ($g_x = 1.9998$, $g_y = 1.9996$, and $g_z = 1.9977$). For the positive polaron, only two contributions were found. These lines are assigned to the two components of the g-tensor, which are either parallel or perpendicular to the external magnetic field ($g_{||} = 2.0029$, $g_{\perp} = 2.0021$). The shape of the line groups was evaluated by computer-driven simulation. From these investigations, we conclude an axial environmental symmetry for the positive polaron on the polymer. For the fullerene anion, we assume a lower, rhombohedric symmetry. Both signals reveal different saturation times. Hence we deduce that both spins appear completely independent of each other, without any spin-exchange correlation.

The application of admittance spectroscopy to ITO/PEDOT:PSS/MDMO-PPV:PCBM/Al devices yielded two frequency-dependent contributions to the device capacitance. For the shallow trap with an activation energy of about 10 meV, no additional DC-bias dependence was observed. We conclude that the thermally activated conductivity originates from this state. The defect with the activation energy of 177 meV is assumed to be located at the interface between the composite layer and the aluminum cathode. A bias independent behavior of the activation energy was observed in our earlier studies [7]. We exclude a bulk defect, since the corresponding activation energy should response to an external DC field due to the Poole-Frenkel effect.

[1] N. S. Sariciftci, Prog. Quant. Electron. **19**, 131 (1995).

[2] W. Rieß, S. Karg, V. Dyakonov, M. Meier, and M. Schwoerer, J. Lum. **60**, 906 (1994).

[3] N. S. Sariciftci, L. Smilowitz, A. J. Heeger, and F. Wudl, Science **258**, 1474 (1992).

[4] V. Dyakonov, G. Zoriniants, M. Scharber, C. J. Brabec, R. A. J. Janssen, J. C. Hummelen, and N. S. Sariciftci, Phys. Rev. B **59**, 8019 (1999).

[5] S. E. Shaheen, C. J. Brabec, N. S. Sariciftci, F. Padinger, and T. Fromhertz, Appl. Phys. Lett. **78**, 841 (2001).

[6] R. Herberholz, M. Igalson, and H. W. Schock, J. Appl. Phys. **83**, 318 (1998).

[7] V. Dyakonov, D. Godovsky, J. Parisi, C. J. Brabec, N. S. Sariciftci, J. C. Hummelen, J. De Ceuster, and E. Goovaerts, Synth. Met. **121**, 1529 (2001).